The 400d X-ray Survey: The Weak Lensing Follow-Up Programme

Holger Israel[1], Thomas Reiprich[1], Thomas Erben[1], Daniel Hudson[1], Peter Schneider[1], Alexei Vikhlinin[2], Craig Sarazin[3], & Kenneth Rines[2]

[1] Argelander-Institut für Astronomie, Auf dem Hügel 71, 53121 Bonn, Germany
[2] Harvard-Smithsonian Center for Astrophysics, 60 Garden Street, Cambridge, MA 02138, USA
[3] Departement of Astronomy, University of Virginia, 530 McCormick Road, Charlottesville, VA 22904, USA

Abstract: Evolution in the mass function of galaxy clusters sensitively traces cosmological structure formation. The number density of massive clusters as a function of z can be used to constrain cosmological parameters. We aim at deriving a robust mass function by a detailed comparison of cluster masses deduced from observations of their X-ray and weak lensing signals. Based on the recent *400d* survey of serendipitous ROSAT detections, we therefore use a complete X-ray flux- and luminosity-limited subsample of clusters at $z \geq 0.35$ for which we conduct a weak lensing follow-up survey. We report first results of our weak lensing analysis based on observations obtained with the MMT Megacam camera.

Cosmology with a New Distant Cluster Sample

Clusters as cosmological probes Galaxy clusters are the most massive and thus most prominent tracers of structure formation. Evolution in their mass function from high to low redshifts provides orthogonal constraints on cosmological parameters compared to CMB or supernova techniques. Its measurement from unbiased, statistically complete samples provides a crucial ingredient for constraining the nature of both dark matter and dark energy. We present a new high-redshift sample for which we are going to compare mass estimates based on X-ray and weak gravitational lensing to arrive at a single mass function in several redshift intervals.

Sample definition Based on the *400d* survey of galaxy clusters serendipitously detected in the complete set of suitable ROSAT PSPC pointings (Burenin et al. 2007), we define a subsample for cosmological studies by the conditions of redshift $z \geq 0.35$ and X-ray luminosity $L_X \geq 10^{44}\mathrm{erg/s}$. The resulting sample consists of 40 galaxy clusters which can be nearly equally distributed in three redshift bins $0.35 \leq z < 0.45$, $0.45 \leq z < 0.55$, and $0.55 \leq z < 0.90$ for which we seek to derive the mass function. While the evolution in their redshift regime is strong, these clusters inhabit a mass range typical for the *local* Universe, and are therefore ideal for a comparison with the *HIFLUGCS* sample at $\bar{z}=0.05$.

Data Reduction

The Data

Our observations have been obtained with the $24' \times 24'$ MEGACAM wide-field imager in Oct. 2004, June 2005, and Oct./Nov. 2005. MEGACAM, a mosaic of 36 CCDs, 2048×4608 pixels each, is located at the 6.5 m MMT telescope at Whipple Observatory, Mt. Hopkins, Arizona.

Observation strategy Lensing analysis is based on deep imaging in the *r'* band aiming at the highest possible number of faint background galaxies suitable for shape measurements. We employ a *dither pattern* to obtain homogeneous data quality throughout the field of view despite gaps between camera chips. Additional *g'* and *i'* imaging will be included to identify cluster members and select catalogues by colours.

Reduction Pipeline and Weak Lensing Analysis

Data reduction is carried out using the THELI pipeline (cf. Erben et al. 2005) designed for processing wide-field data from mosaic cameras. Special care has also been taken to account for the most important premise of weak lensing studies, the accurate retrieval of intensity distribution moments to determine image shapes. For some results presented here a refined, iterative astrometric solution has been used.

Weak lensing information, a catalogue of galaxy positions and ellipticity components $\varepsilon_{1,2}$ is extracted from coadded images using an implementation of the KSB+ algorithm based on the one presented by T. Schrabback in Heymans et al. (2006). Fig. 1 shows that MEGACAM fulfills the necessary condition of the PSF anisotropy being smooth and small.

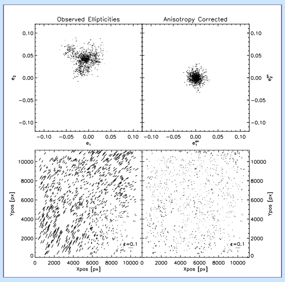

Figure 1: PSF anisotropy correction. Plotted are the ellipticities of sources identified as stars in the coadded image of the CL1701+6414 field (left panels) and their residuals after a subtraction of a quadratic fit function (right panels).

Scatter plots in the upper panels show the distribution of ellipticity components ε_1 and ε_2 before and after anisotropy correction. Note that the modulus of ellipticity for stars effectively vanishes. The *stick plots* in the lower panels show how orientations and magnitudes of PSF anisotropy vary over the imaging plane due to the combination of atmospheric and telescope effects. Owing to the precise alignment of the MEGACAM mosaic and a good astrometric solution, this correlated pattern can easily be removed by fitting a low-order polynomial.

Cluster detection by weak lensing makes use of the *aperture mass statistics* averaging over the tangential ellipticity components $\varepsilon_i^{\mathrm{tan}}$ of galaxies at positions θ_i w.r.t. a given centre θ_0:

$$\hat{M}_{\mathrm{ap}} = \frac{1}{n}\sum_{i=1}^{n} \varepsilon_i^{\mathrm{tan}}(\theta_0) Q(|\theta_i - \theta_0|) \qquad (1)$$

The sum is taken over all galaxies within a suitable filter $Q(\theta)$. With σ_ε the standard deviation of the unlensed ellipticity distribution, clusters are detected as local maxima of the *aperture mass significance*:

$$\frac{S}{N} = \frac{\sqrt{2}}{\sigma_\varepsilon}\frac{\sum_i \varepsilon_i^{\mathrm{tan}}(\theta_0) Q(|\theta_i - \theta_0|)}{\sqrt{Q^2(|\theta_i - \theta_0|)}} \qquad (2)$$

Cluster mass can be inferred by fitting the signal expected from a known mass profile, e.g. the singular isothermal sphere, to the radial shear profile of the detected peak .

First Results

CL0030+2618: Comparing Lensing with X-rays

In a testcase study we compare the weak-lensing mass reconstruction of CL0030+2618 ($z=0.50$) to a CHANDRA analysis (Fig. 2). Using the M_{ap} statistics, the cluster is easily detected with 4.2σ significance applying a polynomial filter introduced by Schneider et al. (1998) at a scale of $\theta_{\mathrm{out}} \approx 4'$. We note that this significance of detection is even higher using the matched filter for cluster detection proposed by Schirmer et al. (2004) at a suitable scale.

Optical images of CL0030+2618 reveal a pronounced overdensity of galaxies centered around two possible cD galaxies separated on the sky by $0.9'$. While the centroid of the X-ray emission by the ICM coincides with the more western of these galaxies which is also close to the centre of curvature of one of the two strong lensing arcs found in this system, the maximal M_{ap} significance is found close to the eastern dominant galaxy.

X-rays While the offset of $\theta \approx 1'$ between X-ray and weak lensing centroids is still consistent with no actual offset, together with the presence of two possible cD galaxies and the overall elongated light distribution it raises the question of the dynamical state of CL0030+2618. It will be interesting to see whether the further analysis of this system reveals more evidence of a possible ongoing merger of two subclumbs. Our next step will be to fit a NFW mass model to the cluster's shear field and to compare the resulting mass to the $M_{\mathrm{tot}} = 4.41^{+2.54}_{-1.69} \cdot 10^{14} M_\odot$ within $r_{180} = 1.638 h_{71}^{-1}\mathrm{Mpc}$ found from the CHANDRA data.

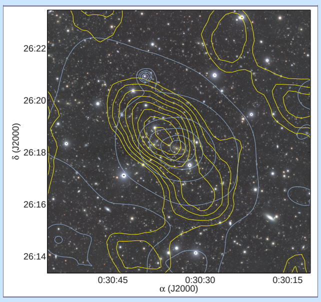

Figure 2: Detections of CL0030+2618. Shown is a composite of the central parts of our coadded *g'*, *r'*, and *i'* images. Overlaid in blue are CHANDRA X-ray contours , while yellow contours give the significance of aperture mass detection, spaced in intervals in S/N of 0.5, starting at $S/N = 0.5$.

CL1701+6414 and CL1641+4001

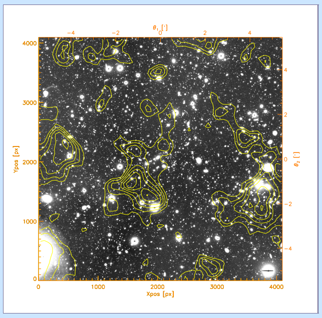

Figure 3: The central $11' \times 11'$ of the coadded *r'*-band image for CL1701+6414 overlaid with the M_{ap} significance contours in intervals in S/N of 0.5, starting at $S/N = 0.5$. The filter from Schirmer et al. (2004) is used at $\theta_{\mathrm{out}} = 4.8'$.

CL1701+6414 Concerning the measurement of its weak lensing signal, CL1701+6414 at $z=0.45$ is an especially interesting, though probably challenging case. Our target cluster (VMF 190, see Vikhlinin et al. 1998) exhibiting a giant arc clearly visible in the coadded image and therefore expected to show a substantial shear signal is only separated by $4.8'$ on the sky from the massive $z=0.22$ cluster Abell 2246 (= VMF 189). In addition, there are two known smaller clusters, VMF 191/192, also at $z=0.22$, in distances of $7.3'$ and $7.9'$ to CL1701+6414 lying roughly *in between* this foreground structure.

This configuration is likely to result in a complicated shear field. To maximise the signal of CL1701+6414, the upper and lower quartile in S/N of galaxies have not been used to exclude both foreground galaxies and the least reliable ellipticities. In a first study, the target cluster (close to the centre of Fig. 3) is best detected at 3.3σ for a filter scale of $\theta_{\mathrm{out}} = 4.8'$, with an offset of $\approx 90''$ to the optical centre, compared to a typical position error for M_{ap} peaks of $\lesssim 60''$. Abell 2246 is clearly detected at 3.1σ to the right side of Fig. 3. We suppose a more refined analysis accounting for this constellation will give more significant detections of both clusters.

For comparison we present in Fig. 4 the weak lensing signal of CL1641+4001 which is at similar redshift ($z=0.46$). We detect it with a maximal significance of 2.7σ using the matched filter at $\theta_{\mathrm{out}} = 8'$ supported by the fact that varying θ_{out} or using the polynomial filter give qualitatively similar results.

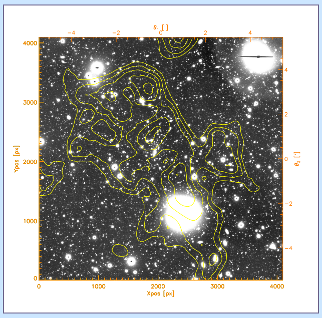

Figure 4: aperture-mass map of the central $11' \times 11'$ of the CL1641+4001 field. Same figure layout as in Fig. 3, but with $\theta_{\mathrm{out}} = 8'$.

Figure 5: Innermost $5.5' \times 5.5'$ of the coadded images for four clusters in our MEGACAM subsample still awaiting lensing analysis: Top left: CL0159+0030 at $z=0.39$. Top right: CL0230+1836 at $z=0.80$. Bottom left: CL1357+6232 at $z=0.53$. Bottom right: CL1416+4446 at $z=0.40$. For the top panel clusters in close proximity ($2.0'$ and $3.6'$) to bright stars ($m_V = 8.3$ each) regions next to the cluster centres will have to be excised from the analysis.

References

Burenin, R. A., Vikhlinin, A., Hornstrup, A., et al.; submitted to ApJS, astro-ph/0610739.
Erben, T., Schirmer, M., Dietrich, J.P., et al.; Astron. Notes 326, 432, (2005).
Heymans, C., van Waerbeke, L., Bacon, D., et al.; MNRAS, 368, 1323, (2006).
Schirmer, M., Erben, T., Schneider, P., et al.; A&A 420, 75, (2004).
Schneider, P., van Waerbeke, L., Jain, B., & Kruse, G.; MNRAS 296, 873, (1998).
Vikhlinin, A., McNamara, B. R., Forman, W., et al.; ApJ 502, 558, (1998).

Contact: hisrael@astro.uni-bonn.de